Supplementary Information for: H_2 in Antarctic firn air: atmospheric reconstructions and implications for anthropogenic emissions

John D. Patterson, Murat Aydin, Andrew M. Crotwell, Gabrielle Pétron, Jeffery P. Severinghaus, Paul B. Krummel, Ray L. Langenfelds, and Eric S. Saltzman

Corresponding author: John D. Patterson Email: jdpatter@uci.edu

This PDF file includes:

Supplementary text

Figs. S1 to S9

Tables S1 and S2

References for SI

Supplementary Information Text

H_2 Measurements

The Megadunes firn air measurements of six trace gases (CO_2, CH_4, N2O, SF_6, CO and H_2) were made at NOAA/GML in April 2004. For this study, we have corrected the reported H_2 data for detector non-linearity, calibration drift, and gravitational fractionation. NOAA/GML H_2 measurements were initially calibrated using a single 530 ppb H_2 standard, assuming a linear detector response. For this study, we have applied an empirical correction to the firn air H_2 data for the non-linear response of the mercuric oxide reduction gas analyzer (HgO-RGA). The non-linearity bias is estimated to be -3 ppb at 453 ppb and -12 ppb at 312 ppb based on a few laboratory measurements made at NOAA/GML in 2009. The biases were linearly interpolated onto the firn air measurements, and the measurements were corrected for the bias (i.e., a measurement of 300 ppb would be corrected to 312 ppb). This correction is identical to the non-linearity correction used in Patterson et al. (1). Similar measurements on a different HgO-RGA showed a non-linearity bias ~ 2 times higher than that reported here (2). It is not known whether such differences in linearity are a function of the specific condition of the two detectors or whether temporal variability in linearity occurs. Because the non-linearity of the NOAA/GML detector was assessed several years after the Megadunes measurements, we cannot rule this out as a source of uncertainty in the correction. Applying the larger non-linearity correction to the firn air data set would increase the H_2 levels in the oldest part of the atmospheric reconstruction by 2-3% (~10 ppb) and have a negligible effect on more recent parts of the record. This uncertainty does not alter the main conclusions of this paper.

The firn air H_2 measurements were originally reported on the NOAA-1996 (NOAA96) calibration scale. The NOAA96 scale drifted over the 1990's, and the World Meteorological Organization recommends reporting H_2 measurements on the MPI09 (also referred to as the WMO H_2 X2009) scale maintained by the Max Plank Institute for Biogeochemistry, Jena, Germany (2). In order to adjust the Megadunes firn air data to the MPI09 scale, we developed an empirical correction based on comparing 2004 surface flask air weekly sample H_2 measurements from Cape Grim made by NOAA/GML to contemporaneous *in situ* high frequency H_2 measurements made by AGAGE reported on the MPI09 scale. Importantly, the empirical corrections presented here are specific for the 2004 Megadunes firn air H_2 data and are based on the best information available to the authors at this time. NOAA/GML is in the process of

adopting the MPI09 scale for its more recent measurements (2010 forward) and may revise older H_2 records in the future. The firn air flasks were analyzed for H_2 at NOAA/GML in April 2004. During the same time period, Cape Grim surface air samples from January-March 2004 were also analyzed by NOAA/GML. The average offset between the AGAGE measurements and the NOAA/GML measurements during these months is 1.6 ppb (with AGAGE measurements higher than NOAA/GML measurements). We applied a constant correction of 1.6 ppb (0.3% at 500 ppb) to all of the firn air measurements. An analogous approach was used to derive an empirical correction to adjust the NOAA/GML flask air H_2 measurements from high southern latitudes from the NOAA96 scale to the MPI09 scale (Figure S1; refs. 3–5). A time-dependent correction was applied to the NOAA/GML flask air H_2 measurements based on the difference between the Cape Grim H_2 measurements from NOAA/GML and AGAGE.

H_2 measurements from Cape Grim made by AGAGE (*in situ*) and measurements made by CSIRO (flask) show a small but significant increase in atmospheric H_2 during the 1990's in the high southern latitudes (Figure S1; refs. 5, 6). This trend has not previously been discussed in the literature. It is supported by data from Khalil & Rasmussen (7) who reported an increase from 510 to 518 ppb of H_2 in the high southern latitudes between 1985 and 1989. The relationship between the calibration scale of Khalil & Rasmussen (7) and MPI09 is uncertain. The implied trend in atmospheric H_2 from 1989-1992 is dependent on the relationship between the two calibration scales, but the observed increase in atmospheric H_2 from 1985-1989 is independent of that relationship, provided that the Khalil & Rasmussen (7) calibration was reasonably stable over that time. The NOAA/GML flask measurements also show an increasing trend during the 1990's after adjustment to the MPI09 scale, but that is because the calibration adjustment is tied to the measurements from AGAGE. Both AGAGE and CSIRO data are calibrated against the implementation of the MPI09 scale maintained by CSIRO. The H_2 trend through the 1990s into the early 2000s is constrained by relative stability among a large number of high-pressure cylinders, mostly containing natural, background Southern Hemisphere air, including 15 individual cylinders first analyzed between 1992 and 1996, and monitored over 7+ years, with relative stability better than ±0.2 ppb y^{-1} (8). An earlier description of CSIRO's H_2 calibration was provided by Francey et al. (8).

The firn air measurements were also corrected for gravitational fractionation. Gravitational fractionation describes the process by which heavier species are progressively

enriched with depth in the firn, and is described by the barometric equation (9, 10). We applied an empirical correction by scaling $\delta^{15}N$ data from the same borehole according to equation S1:

$$Corr_{grav}(z) = \frac{\delta^{15}N(z)}{1000} * \frac{\exp\left(g*z*\frac{\Delta m_{H2}}{RT}\right)-1}{\exp\left(g*z*\frac{\Delta m_{15N}}{RT}\right)-1} \quad \text{(S1)}$$

Where $Corr_{grav}$ is the depth dependent fractional correction for H_2, $\delta^{15}N$ is the measured nitrogen isotopic abundance at each depth (‰), g is the gravitational acceleration constant (9.8 m s^{-2}), z is depth (m), R is the ideal gas constant (8.314 J mol^{-1} K^{-1}), T is the annual average temperature at Megadunes (224 K), Δm_{H2} is the difference in molar mass between H_2 and air (.0270 kg), and Δm_{15N} is the difference in molar mass between $^{28}N_2$ and $^{29}N_2$ (.001 kg). The maximum gravitational correction for the H_2 data is .77% at 67.4 m. Similar corrections were applied to the CO_2 and CH_4 firn air data using the difference in molar mass between each gas and air. Duplicate measurements from the same depth are then averaged. The corrected, depth-averaged profile shows an approximately linear increase in H_2 levels from 360 ppb at 68.5 m to 550 ppb at 63.4 m (Figure S2b). Above 63.4 m, H_2 levels are approximately constant at 550 ppb near modern high southern latitude levels.

Estimating the H_2 Budget

The 2003 budget was estimated largely from Pieterse et al. (11). The sources and sinks were distributed primarily according to Price et al. (12). Variations in source strength between 1852 and 2003 were estimated as described below, first-order loss rates were assumed to be constant in time. The box model solves for steady state.

Sources

CH_4 oxidation: Atmospheric CH_4 concentration is prescribed from Dlugokencky (13) and Etheridge et al. (14). The distribution and concentration of OH is prescribed from Spivakovsky et al. (15). The temperature dependent rate constant of the reaction of OH with CH_4 is calculated from Burkholder et al. (16). H_2 yields from the oxidation of CH_4 by OH are from Novelli et al. (3).

Anthropogenic H_2: This source includes both direct anthropogenic emissions and oxidation of anthropogenic NMHCs. Total anthropogenic H_2 is prescribed to be 18.8 Tg in 2003. Of this, 17 Tg were direct emissions after Pieterse et al. (11). The contribution from anthropogenic NMHC oxidation (1.8 Tg) was estimated by subtracting the calculated CH_4 oxidation source from the total photochemical production of Pieterse et al. (11). The remaining photochemical source is partitioned between biogenic NMHC and anthropogenic NMHC oxidation using Ehhalt & Rohrer (17). An H_2/CO molar emissions ratio of .23 was calculated from total CO emissions of 1,147 Tg in 2003 after Verhulst (18). The source was scaled in time using the historical CO budget of Verhulst (18), assuming a constant emissions ratio. Emissions are distributed according to Price et al. (12). An analogous method using the CO_2 emissions inventory of Boden et al.(19) was used for a scenario with monotonically increasing anthropogenic H_2 (Figure S7).

Biomass burning: Total biomass burning emissions of H_2 are prescribed to be 15 Tg in 2003 after Pieterse et al. (11). An H_2/CO molar emissions ratio of .46 was calculated from total CO emissions of 459 Tg after Lamarque et al. (20) and Verhulst (18). Biomass burning emissions were scaled in time using the historical CO emissions inventory of Lamarque et al. (20) assuming a constant emissions ratio. Biomass burning emissions are distributed according to Price et al. (12).

Biogenic NMHC oxidation: The total biogenic NMHC oxidation source is prescribed to be 12.2 Tg y^{-1}. The magnitude of the source is estimated by subtracting the calculated CH_4 oxidation source from the total photochemical production of Pieterse et al. (11). The remaining photochemical source is partitioned between biogenic NMHC and anthropogenic NMHC oxidation using Ehhalt & Rohrer (17). The source is distributed using the gridded biogenic NMHC emissions inventory of Sindelarova et al. (21). The biogenic source is assumed constant in time.

N_2 fixation-oceans: Total production of H_2 in the surface ocean is estimated using global marine N_2 fixation of 150 Tg y^{-1} and 1:1 molar stoichiometry (12, 22). It is distributed according to Deutsch et al. (23). Ocean-atmosphere exchange is parameterized using the method of Butler (24). The H_2 loss constant is assumed to be uniform in each box, and it is tuned to yield the same

ocean-atmosphere flux as Pieterse et al. (11) for the year 2003. The transfer velocity is dependent on temperature, salinity, wind speed, and, humidity for each box and is calculated from Fairall et al. (25). The ocean model includes latitude-dependent mixed layer depths. All parameters (except atmospheric H_2) are identical between 1852 and 2003.

N_2 fixation-terrestrial: H_2 emissions from terrestrial biological N_2 fixation are prescribed. For the year 2003, the emissions of Pieterse et al. (11) are used. Between 1852 and 2003, emissions are assumed to scale with historical biological N_2 fixation from Fowler et al. (26). The emissions are distributed using the gridded estimates of NPP from the MODIS satellite (27).

Sinks

Soil microbial respiration: The soil microbial sink is assumed to be first order, and the rate constant is calculated from Pieterse et al. (i.e. flux/burden; ref. 11). The soil sink is distributed according to Price et al. (12).

OH oxidation: The distribution and concentration of OH is prescribed from Spivakovsky et al. (15). The temperature dependent rate constant of the oxidation of H_2 by OH is calculated from Burkholder et al. (16).

Stratospheric loss: The first order stratospheric loss constant is estimated from Xiao et al. (28).

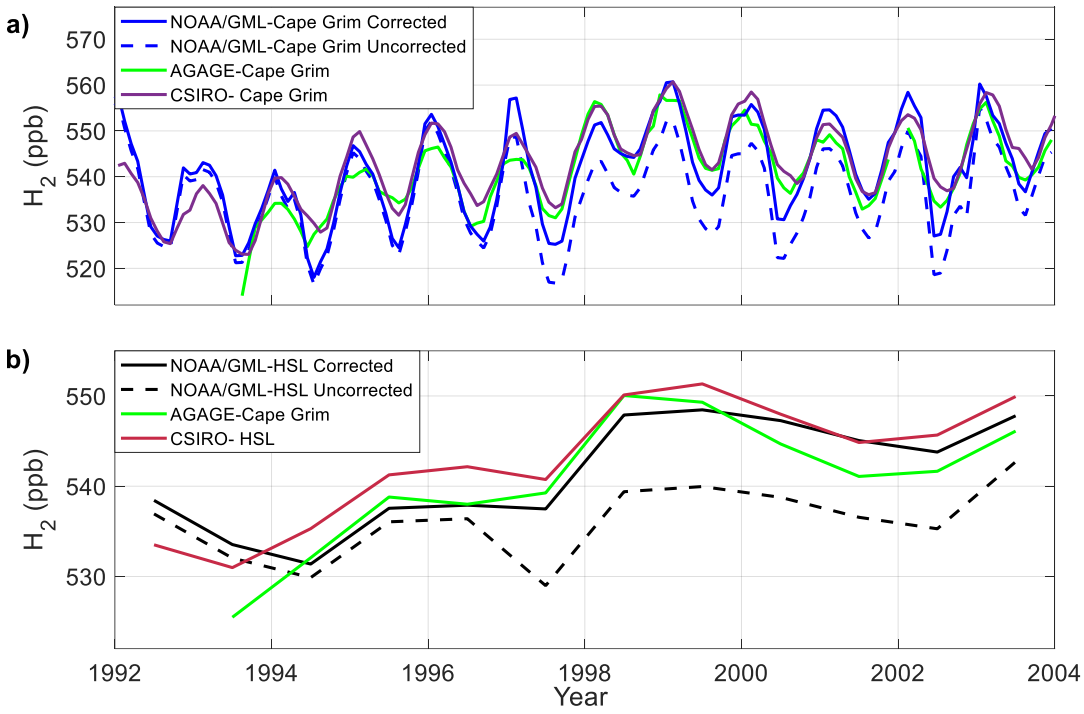

Fig. S1. Modern observations of atmospheric H_2 a) Atmospheric H_2 monthly means from Cape Grim, Tasmania, observations: dashed blue line- uncorrected measurements from NOAA/GML; solid blue line- measurements from NOAA/GML corrected to the MPI09 calibration scale as described in the text, solid green line- *in situ* measurements from AGAGE, solid purple line-flask air measurements from CSIRO (3–6); b) Annually averaged atmospheric H_2: dashed black line- uncorrected NOAA/GML measurements averaged from all high southern latitude (HSL) flask collection sites including Palmer, Syowa, South Pole, and Halley stations, Antarctica and Cape Grim Observatory, Tasmania, solid black line- NOAA/GML measurements averaged from all high southern latitude flask collection sites corrected to the MPI09 calibration scale, solid green line- *in situ* measurements from AGAGE at Cape Grim, solid maroon line CSIRO measurements averaged from all high southern latitude flask collection sites including Casey, South Pole, and Mawson Stations, Antarctica, and Cape Grim and Macquarie Island, Tasmania.

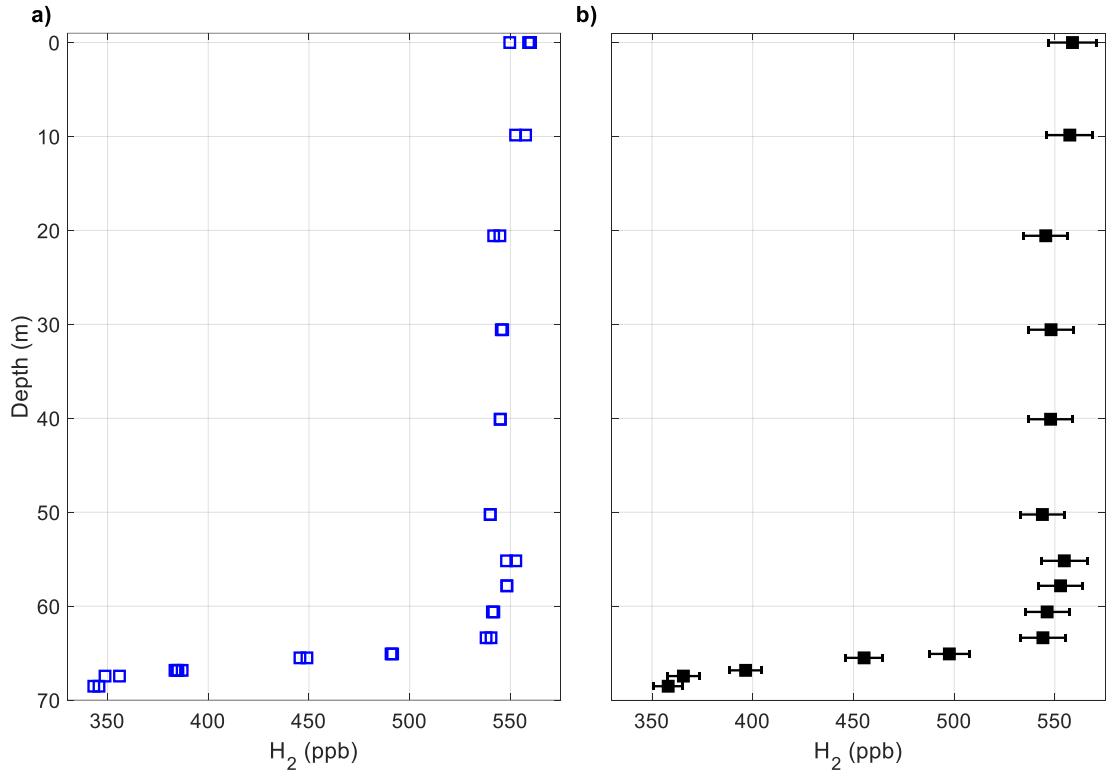

Fig. S2. Measured depth profile of H_2 in Megadunes firn air a) Raw measurements of H_2 from the 2004 Megadunes firn air sampling expedition b) Depth- averaged H_2 measurements after correcting for the non-linear response of the HgO-RGA, calibration offset, and gravitational fractionation also shown in Figure 1B. Error bars are ±1σ including the propagated 2% analytical uncertainty.

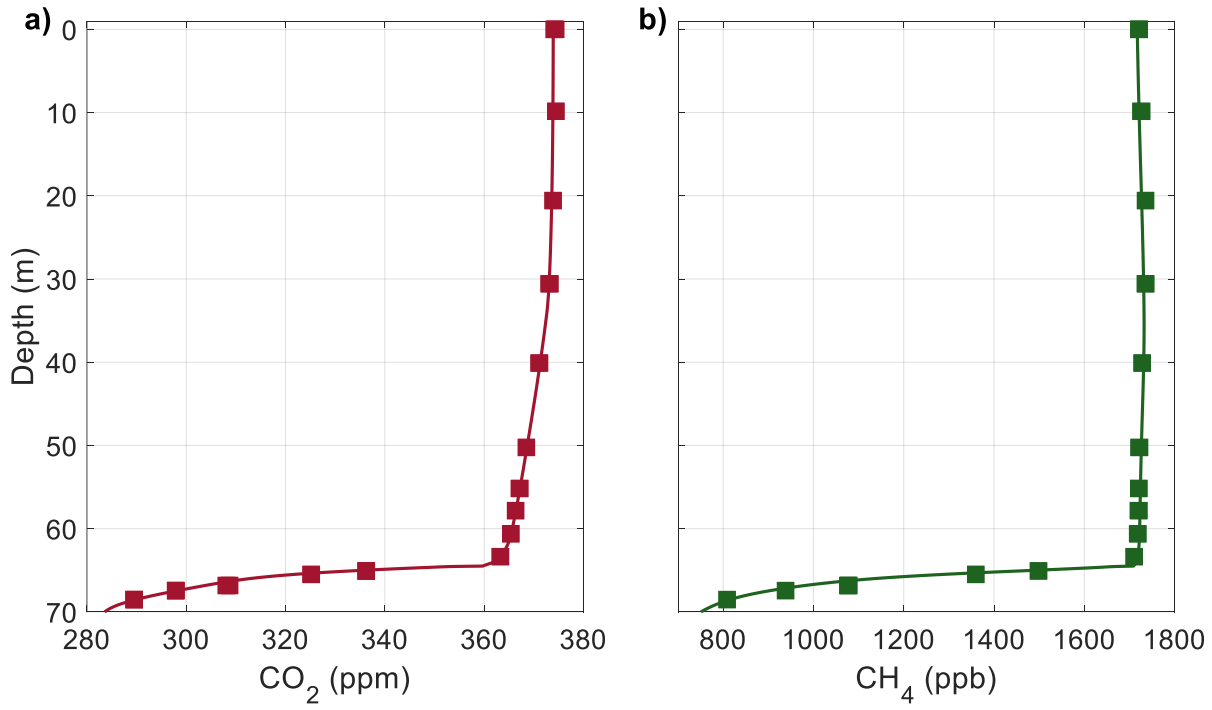

Fig. S3. Measured and modeled depth profiles at Megadunes for a) CO_2 and b) CH_4. Solid lines are the model result and squares are measurements. The measurements have been corrected for gravitational fractionation as described by equation S1. The model was forced using atmospheric histories based on high resolution ice core measurements from Law Dome and modern flask air measurements from NOAA/GML (13, 14, 29, 30)

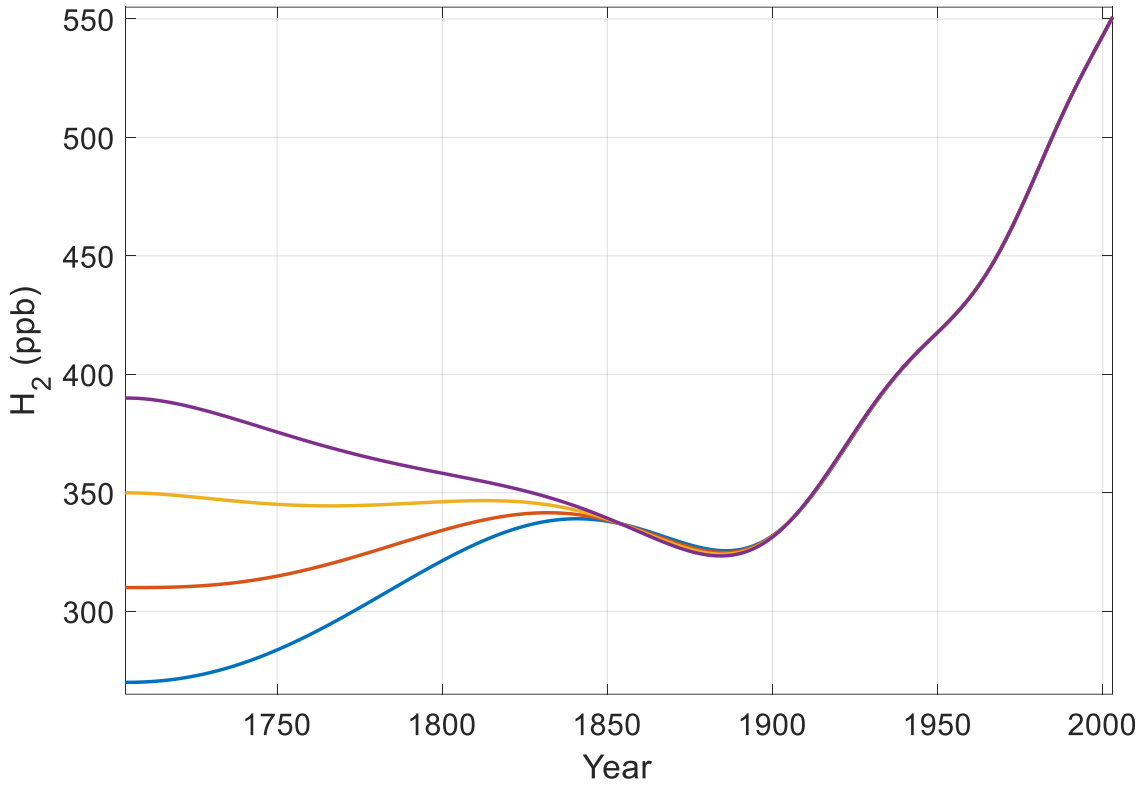

Fig. S4. Inversion result for each assumed "preindustrial" baseline. Each line is the average of 1000 Monte Carlo runs using $\alpha = 8*10^{-2}$ (see text). Prior to 1852, the inversion result is sensitive to the assumed preindustrial baseline. After 1852, the results converge, and the sensitivity to the preindustrial baseline is greatly reduced.

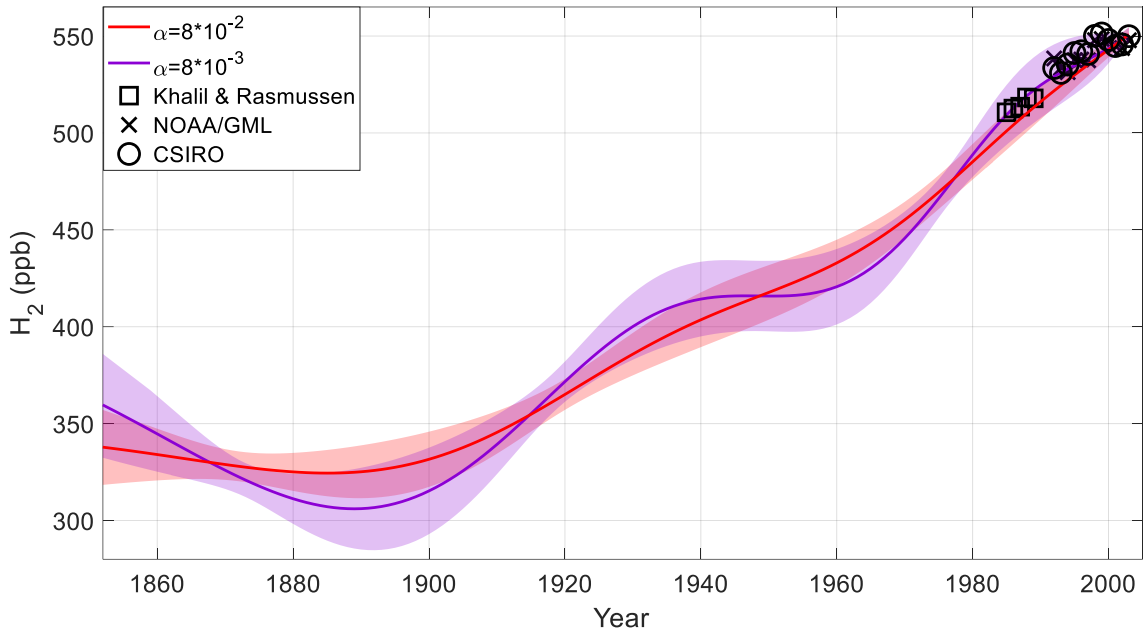

Fig. S5. Atmospheric history of H_2 since 1852 inferred from Megadunes firn air: red line and shading – mean atmospheric history and ±1σ uncertainty from 4000 Monte-Carlo runs using $\alpha = 8*10^{-2}$ (see text); purple line and shading- mean atmospheric history and ±1σ uncertainty from 4000 Monte-Carlo runs using $\alpha = 8*10^{-3}$; black squares, x's, and circles – atmospheric H_2 annual means from high southern latitude sites from 1985-1989 and 1992-2003 (3, 4, 6, 7). The same general trends are present in both inversion results, and the differences between the two histories are not important for the main conclusions of this work. A slight decrease in H_2 levels during the late 19th century and a plateau in the mid-20th century is present in the inversion results using $\alpha = 8*10^{-3}$. These features should not be considered robust until they can be confirmed with high resolution ice core measurements. We note that the inversion results with $\alpha = 8*10^{-3}$ produces slightly better agreement to modern flask measurements. Using $\alpha < 8*10^{-3}$ yields unrealistic high frequency fluctuations in the inversion results and in deteriorating agreement between the inversion result and modern flask measurements. Using $\alpha > 8*10^{-2}$ yields deteriorating agreement between the modeled and measured depth profiles.

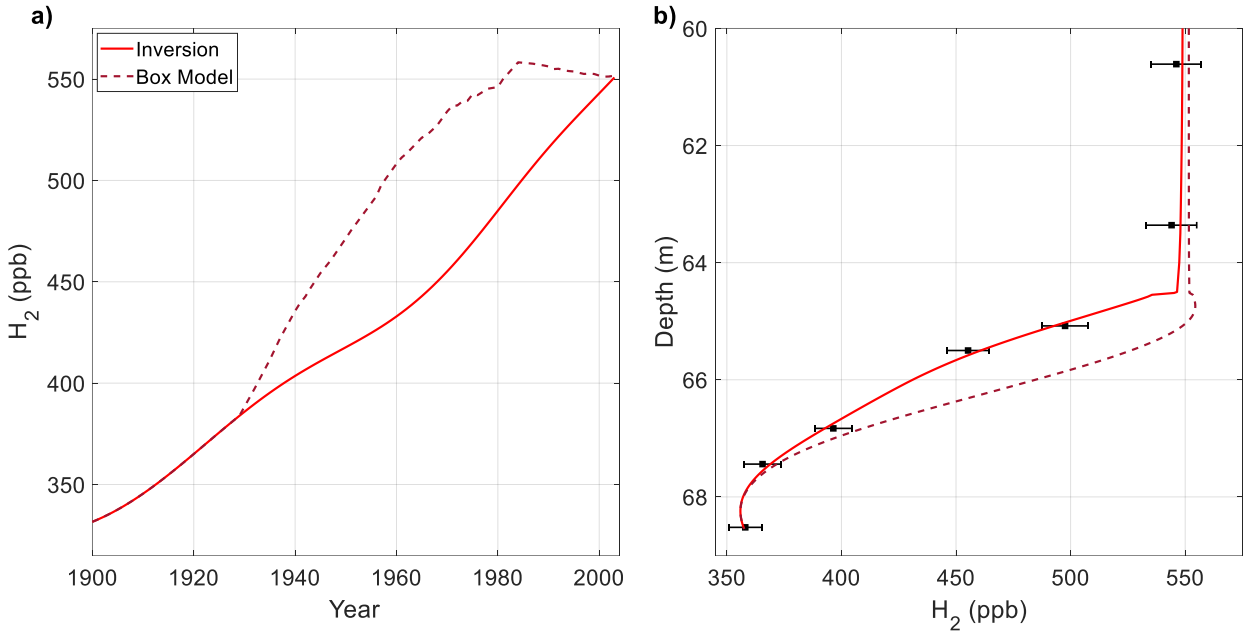

Fig. S6. Comparison of atmospheric histories of H_2 with a late 20th century rise and a late 20th century plateau and associated modeled depth profiles a) solid red line- atmospheric history of H_2 since 1852 inferred from Megadunes firn air (mean of 4000 Monte Carlo runs as in Figure 1A), dashed maroon line- adapted history from the box model using the historical budget based on Verhulst (2014). Before 1930, the history is identical to the firn air derived history. After 1930, the history is the result from the 60^o-90^o S box in the six-box model as in Figure 4C; b) black squares and error bars- Megadunes firn air H_2 measurements as in Figure 1A, solid red line and dashed maroon line- modeled depth profiles resulting from the atmospheric histories in (a). A rapid rise from 1920 to 1985 and subsequent slow decrease in atmospheric H_2 yields much worse agreement with the firn H_2 measurements between 64 and 67 m than a slower, steady increase from 1900-2003.

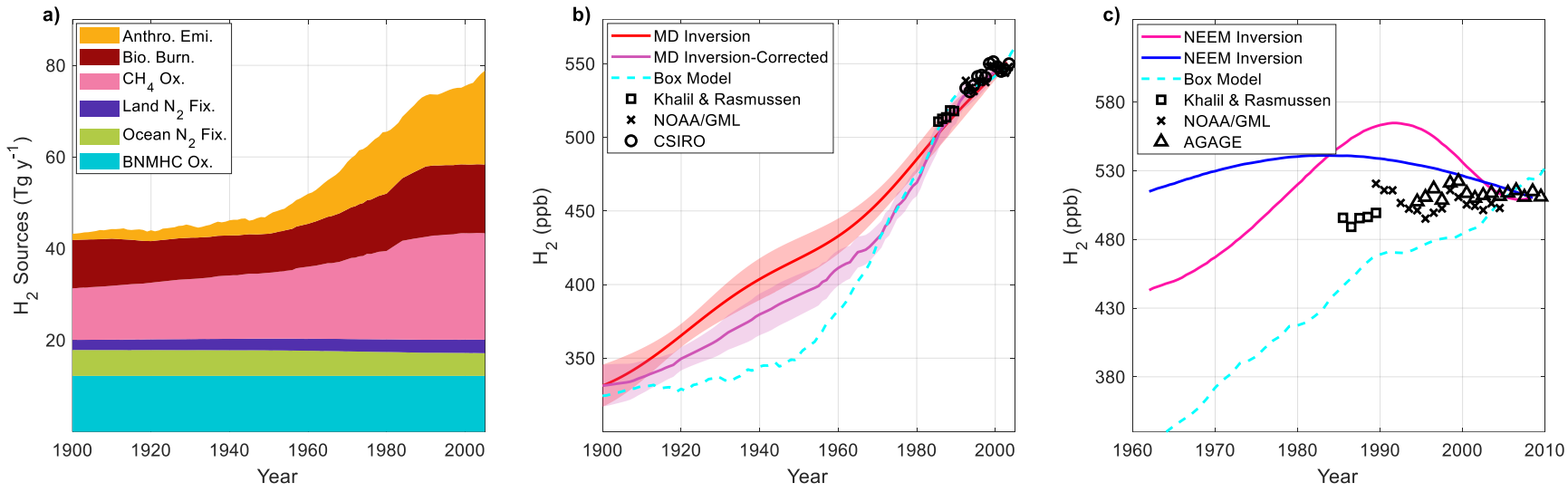

Fig. S7. Results from the investigation of changes to the budget of atmospheric H_2 using a box model. a) historical budget used for the box modelling exercise, based primarily on Pieterse et al. and Boden et al. (11, 19). The only difference between the budget in (a) and in Figure 4A is the anthropogenic H_2, which was scaled with the inventory of anthropogenic CO_2 from Boden et al. (19) instead of the CO emissions of Verhulst (18). b) red and purple lines and shading- firn air reconstructions for Antarctic H_2 as in Figure 4C, dashed cyan line- atmospheric mixing ratio in the 60°-90° S box from the box model corresponding to the historical budget shown in (a). c) black and magenta lines- northern hemisphere atmospheric histories of H_2 from Petrenko et al. as in Figure 4D, black squares, black x's, and black triangles – observed atmospheric H_2 annual means from high northern latitude sites as in Figure 4D (2, 13, 17,

19), dashed cyan line- atmospheric mixing ratio in the 60^{o}-90^{o} N box from the box model corresponding to the historical budget shown in (a). Forcing the box model with monotonically increasing anthropogenic emissions produces much better agreement to the Antarctic firn air atmospheric histories and flask measurements, than forcing the model with the emissions in Figure 4A during the late 20th century. There are large discrepancies between the northern hemisphere atmospheric histories, flask measurements, and box model result.

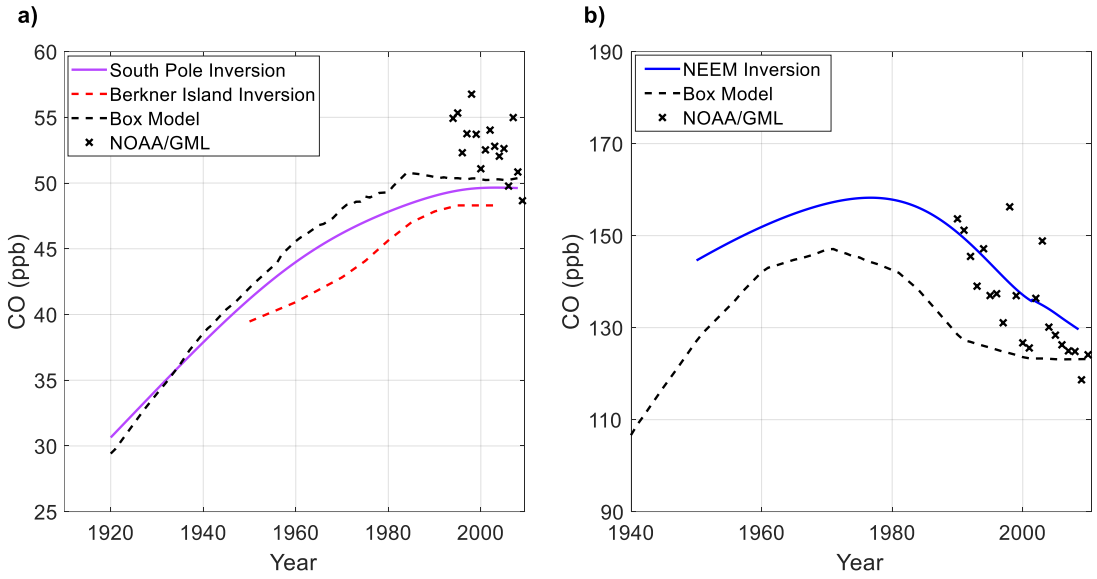

Fig. S8. Comparison of atmospheric CO flask measurements, reconstructions, and results from the six-box model when it is forced with the historical budget of Verhulst (18), a) purple line-atmospheric history derived from South Pole firn air (18), red dashed line-atmospheric history derived from Berkner Island firn air (31), black dashed line- atmospheric mixing ratio in the 60°-90° S box from the box model using the historical budget of Verhulst (18), black x's- observed atmospheric CO annual means a high southern latitude sites (32); b) blue line- atmospheric history from NEEM firn air (33), black dashed line- atmospheric mixing ratio in the 60°-90° N box from the box model using the historical budget of Verhulst (18), black x's- observed atmospheric CO annual means a high northern latitude sites (32). The results from the box model for the southern hemisphere show good agreement with the firn air derived atmospheric histories. Box model results from the northern hemisphere demonstrate similar trends to the firn air derived atmospheric histories but are biased low by ~10%. This bias is likely attributable to transport processes that are not resolved in our six-box model. Small scale transport processes

are more important for CO than H_2 because of its much shorter atmospheric lifetime (2 months for CO and 2 years for $H_{2)}$. The historical budget of Verhulst (18) generates good agreement to the firn air derived histories when it is used to force a more sophisticated 3d atmospheric chemical transport model (18).

Fig. S9. Locations of Megadunes and South Pole drill sites in Antarctica.

Table S1- Estimates of the modern budget of atmospheric H_2 from several references. The last two columns are the budget used to force the six-box model in the years 1900 and 2003. The 2003 budget was developed largely from Pieterse et al. (11).

	Novelli et al. (3)	**Price et al.** (12)	**Ehhalt & Rohrer** (17)	**Pieterse et al.** (11)	**1900 (This Study)**	**2003 (This Study)**
Sources (Tg y^{-1})						
Anthropogenic emissions[a]	15 ± 10	22.7	11 ± 4	$17.0\pm^{3}_{6}$	0 (1.4)[b]	17.0
Biomass burning	16 ± 5	10.1	15 ± 6	15 ± 5	10.5	15.0
Land N_2 fixation	3 ± 1	0	3 ± 2	$3.0\pm^{3}_{3}$	2.2	3.0
Ocean N_2 fixation	3 ± 2	6.0	6 ± 3	$5.0\pm^{3}_{2}$	5.7	5.0
Photochemical production	40	34.3	41 ± 11	37.3	23.5	37.3
From CH_4	26 ± 9	24.5	23 ± 8		11.3	23.3
From NMHCs[c]	14 ± 7	9.8	18 ± 7		12.2	14.0[c]
Total	**77 ± 16**	**73**	**76 ± 14**	**77.3**	**41.9 (43.3)[b]**	**77.3**
Sinks (Tg y^{-1})						
Soil uptake	56 ± 41	55	$60\pm^{30}_{20}$	55.8	29.9 (30.9)[b]	55.5
OH oxidation	19 ± 5	18	19 ± 5	22.1	11.3 (11.6)[b]	20.4
Stratospheric Losses					.7 (.7)[b]	1.3
Total	**75 ± 41**	**73**	$\mathbf{79\pm^{30}_{20}}$	**77.9**	**41.9 (43.2)[b]**	**77.2**

[a] Includes only direct emissions from fossil fuel and biofuel burning
[b] Parenthesized numbers are for CO_2 based anthropogenic H_2 (Figure S7)
[c] Includes biogenic and anthropogenic NMHCs

Table S2- Estimates of the share of the budget accounted for by each source and sink for CO and H_2. Source shares are very similar for the two gases, but sink shares are very different.

	CO: Duncan (34)	**CO: Verhulst** (18)	**H_2: This work**
Sources (share of total sources)			
Anthropogenic emissions[a]	28 %	38 %	24 %
Biomass burning	22 %	15 %	19 %
Land N_2 fixation	0 %	0 %	4%
Ocean Emissions	0 %	1 %	6 %
Photochemical production	51 %	45 %	48 %
From CH_4	35 %	28 %	30 %
From biogenic NMHCs	16 %	17 %	16 %
Sinks (share of total sinks)			
Soil uptake	10 %	8 %	72 %
OH oxidation	90 %	92 %	26 %
Stratospheric Losses	0 %	0 %	2 %

[a] Includes direct emissions from fossil fuels and biofuel burning and photochemical production from anthropogenic NMHCs

References

1. J. D. Patterson, *et al.*, Atmospheric History of H2 Over the Past Century Reconstructed From South Pole Firn Air. *Geophys. Res. Lett.* **47**, 1–8 (2020).

2. A. Jordan, B. Steinberg, Calibration of atmospheric hydrogen measurements. *Atmos. Meas. Tech.* **4**, 509–521 (2011).

3. P. C. Novelli, *et al.*, Molecular hydrogen in the troposphere: Global distribution and budget. *J. Geophys. Res.* **104**, 30427–30444 (1999).

4. P. C. Novelli, Atmospheric Hydrogen Mixing Ratios from the NOAA GMD Carbon Cycle Cooperative Global Air Sampling Network, 1988-2005. *NOAA/ESRL* (2006).

5. R. G. Prinn, *et al.*, History of chemically and radiatively important atmospheric gases from the Advanced Global Atmospheric Gases Experiment (AGAGE). *Earth Syst. Sci. Data* **10**, 985–1018 (2018).

6. R. L. Langenfelds, *et al.*, Interannual growth rate variations of atmospheric CO2 and its δ13C, H2, CH4, and CO between 1992 and 1999 linked to biomass burning. *Global Biogeochem. Cycles* **16** (2002).

7. M. A. K. Khalil, R. A. Rasmussen, Global increase of atmospheric molecular hydrogen. *Nature* **347**, 743–745 (1990).

8. R. J. Francey, *et al.*, "The CSIRO (Australia) measurement of greenhouse gases in the global atmosphere" (2003).

9. H. Craig, Y. Horibe, T. Sowers, Gravitational Separation of Gases and Isotopes in Polar Ice Caps. *Science (80-.).* **242**, 1675–1678 (1988).

10. M. L. Bender, T. Sowers, J. M. Barnola, J. Chapellaz, Changes in the O2/N 2 ratio of the atmosphere during. *Geophys. Res. Lett.* **21**, 189–192 (1994).

11. G. Pieterse, *et al.*, Global modelling of H2 mixing ratios and isotopic compositions with the TM5 model. *Atmos. Chem. Phys.* **11**, 7001–7026 (2011).

12. H. Price, *et al.*, Global budget of molecular hydrogen and its deuterium content: Constraints from ground station, cruise, and aircraft observations. *J. Geophys. Res. Atmos.* **112**, 1–16 (2007).

13. E. Dlugokencky, X. Lan, Atmospheric Methane Dry Air Mole Fractions from the NOAA GML Carbon Cycle Cooperative Global Air Sampling Network, 1983-2019. *NOAA/ESRL* (2020).

14. D. M. Etheridge, L. P. Steele, R. J. Francey, R. L. Langenfelds, Atmospheric methane between 1000 A.D. and present: Evidence of anthropogenic emissions and climatic variability. *J. Geophys. Res.* **103**, 15,979-15,993 (1998).

15. C. M. Spivakovsky, *et al.*, Three-dimensional climatological distribution of tropospheric OH: Update and evaluation. *J. Geophys. Res. Atmos.* **105**, 8931–8980 (2000).

16. J. B. Burkholder, *et al.*, "Chemical Kinetics and Photochemical Data for Use in Atmospheric Studies Evaluation Number 18" (2015).

17. D. H. Ehhalt, F. Rohrer, The tropospheric cycle of H2: A critical review. *Tellus, Ser. B Chem. Phys. Meteorol.* **61**, 500–535 (2009).

18. K. R. Verhulst, "Atmospheric Histories of Ethane and Carbon Monoxide from Polar Firn Air and Ice Cores." (2014).

19. T. A. Boden, G. Marland, R. J. Andres, "Global, Regional, and National Fossil-Fuel CO2 Emissions" (2017).

20. J. F. Lamarque, *et al.*, Historical (1850-2000) gridded anthropogenic and biomass burning emissions of reactive gases and aerosols: Methodology and application. *Atmos. Chem. Phys.* **10**, 7017–7039 (2010).

21. K. Sindelarova, *et al.*, Global data set of biogenic VOC emissions calculated by the MEGAN model over the last 30 years. *Atmos. Chem. Phys.* **14**, 9317–9341 (2014).

22. T. D. Brock, M. T. Madigan, *Biology of microorganisms*, 6th Ed. (Prentice-Hall, 1991).

23. C. Deutsch, J. L. Sarmiento, D. M. Sigman, N. Gruber, J. P. Dunne, Spatial coupling of nitrogen inputs and losses in the ocean. *Nature* **445**, 163–167 (2007).

24. J. H. Butler, The potential role of the ocean in regulating atmospheric CH3Br. *Geophys. Res. Lett.* **21**, 185–188 (1994).

25. C. W. Fairall, *et al.*, Implementation of the Coupled Ocean-Atmosphere Response Experiment flux algorithm with CO2, dimethyl sulfide, and O3. *J. Geophys. Res. Ocean.* **116** (2011).

26. D. Fowler, *et al.*, The global nitrogen cycle in the twenty-first century. *Philos. Trans. R. Soc. B Biol. Sci.* **368** (2013).

27. S. Running, Q. Mu, M. Zhao, "MOD17A3 - MODIS/Terra Gross Primary Productivity Yearly L4 Global 1km SIN Grid" (2015) https:/doi.org/10.5067/MODIS/MOD17A3.006.

28. X. Xiao, *et al.*, Optimal estimation of the soil uptake rate of molecular hydrogen from the Advanced Global Atmospheric Gases Experiment and other measurements. *J. Geophys. Res. Atmos.* **112**, 1–15 (2007).

29. D. M. Etheridge, L. P. Steele, R. L. Langenfelds, R. J. Francey, Natural and anthropogenic changes in atmospheric CO 2 over the last 1000 years from air in Antarctic ice and firn. *J. Geophys. Res.* **101**, 4115–4128 (1996).

30. E. Dlugokencky, X. Lan, Atmospheric Carbon Dioxide Dry Air Mole Fractions from the NOAA GML Carbon Cycle Cooperative Global Air Sampling Network, 1968-2019. *NOAA/ESRL* (2020).

31. S. S. Assonov, *et al.*, Evidence for a CO increase in the SH during the 20th century based on firn air samples from Berkner Island, Antarctica. *Atmos. Chem. Phys.* **7**, 295–308 (2007).

32. G. Petron, *et al.*, Atmospheric Carbon Monoxide Dry Air Mole Fractions from the NOAA GML Carbon Cycle Cooperative Global Air Sampling Network, 1988-2020, Version: 2020-08 (2020) https:/doi.org/https://doi.org/10.15138/33bv-s284.

33. V. V. Petrenko, *et al.*, A 60 yr record of atmospheric carbon monoxide reconstructed from Greenland firn air. *Atmos. Chem. Phys.* **13**, 7567–7585 (2013).

34. B. N. Duncan, *et al.*, Global budget of CO, 1988 - 1997: Source estimates and validation with a global model. *J. Geophys. Res. Atmos.* **112**, 1988–1997 (2007).